PNAS
www.pnas.org

Supplementary Information for

Defining the Layers of a Sensory Cilium with STORM and Cryo-Electron Nanoscopy

Michael A. Robichaux, Valencia L. Potter, Zhixian Zhang, Feng He, Jun Liu, Michael F. Schmid, Theodore G. Wensel

Theodore G. Wensel
Email: twensel@bcm.edu

This PDF file includes:

www.pnas.org/cgi/doi/10.1073/pnas.1902003116

SUPPLEMENTARY TEXT

Extended Materials and Methods

Animals

All wild-type mice used for this study were C57BL/6 between ages 3 weeks and 3 months. For STORM immunostaining conditions, at least 3 WT mouse replicates were used; N-values in the text represent the number of individual rod cilia/connecting cilia analyzed per condition. Examples of replicate STORM images are provided for all conditions in the Supplemental Information, and replicate information including number of mouse replicates and number of cilia analyzed by STORM is described in Table S1. *Bbs2*$^{-/-}$ and *Bbs7*$^{-/-}$ mutant backcrossed C57BL/6 strains were acquired from the Jackson Laboratory (*Bbs2* – stock no. 010727, *Bbs7* – stock no. 24979) *BBS4*$^{-/-}$ mice (also C57BL/6) were acquired from Dr. Samuel Wu. Heterozygous crosses were bred to produce homozygous knockouts from each strain as determined by mouse tail genotyping. *Bbs5*$^{flox/flox}$ conditional mice (*C57BL/6N-Bbs5*$^{tm1c(EUCOMM)Wtsi/H}$), which contain *loxP* sites flanking exons 4 and 5, were generated by the European Conditional Mouse Mutagenesis Program (EUCOMM) and acquired from Medical Research Council (MRC) Harwell, Didcot, United Kingdom (stock #09033). *BBS5*$^{flox/flox}$ animals were bred to opsin-promoter *iCre75* mice in a C57BL/6 background to generate rod cell specific knockouts. Biological replicate information regarding *Bbs* mutant experiments are described in Table S1. All procedures adhered to the NIH Guide for the Care and Use of Laboratory Animals, and were approved by the Baylor College of Medicine Institutional Animal Care and Use Committee.

Cryo-ET

Rod cell fragments containing outer segments, CC, and portions of the IS were collected from WT mice by iso-osmotic density-gradient centrifugation as described previously (1, 2). A suspension of cells in Ringer's buffer (20 µL) was mixed with 8 µL of BSA-stabilized 15 nm fiducial gold (Electron Microscopy Sciences), and 2.5 µL of the mixture was applied to a pre-cleaned, glow-discharged 200 mesh Quantifoil carbon-coated holey grids. Samples were plunge-frozen in liquid ethane held at liquid nitrogen temperature using a Vitrobot Mark III automated plunge-freezing device. The frozen-hydrated specimen were imaged at -180 °C in a Polara G2 electron microscope (FEI Company), equipped with a field emission gun and a direct detection device (Gatan K2 Summit). Using SerialEM80 (3). Images were collected at magnifications of 9,400 x at 300 kV with a defocus of ~9 µm; pixel size at the specimen was 4.5 Å. Single-axis tilt series were collected with a cumulative dose of ~50 e−/Å2 distributed over 35 stacks covering an angular range of -51° to +51° with 3° increments. Each stack contained ~8 images and Motioncorr (4) was used to correct image drift within each stack. Alignment and 3D reconstruction were performed using IMOD (5, 6). A total of 20 reconstructions were generated. Of these, only one (Fig. 1A-H) had a CC cross-section with a low enough axial ratio for sub-tomogram averaging, i.e. ≤ 1.31:1. Five others were used to search extensively for cilium- and basal-body associated features, such as "transition fibers" and to generate figures illustrating selected features. For visualization, these were binned 4-fold (Fig.1Ic-d) or 8-fold (Fig.1Ia) to a voxel dimension of 17.8 Å or 35.6 Å, respectively, and subjected to 150 Å low-pass filtering using EMAN2 to reduce the high-frequency noise and make it easier to visualize surfaces and boundaries. (7). Manual volume

segmentation was performed with Scripts (e2maskimod.py) from EMAN2 software package and IMOD (5), and visualized using UCSF Chimera (8).

Subtomogram averaging was carried out as described previously (9). The averaging procedure used was 1) the axis of the cilium was aligned along z, and centered in the x and y directions; where there was a bend in the cilium, the base was used for this centering. 2) the ellipticity of the cilium was measured (major and minor axes). 3) the cilium was rotated so the major and minor axes were along the x or y axis of the tomogram. 4) the minor axis was "stretched" into a circle by rescaling along one of the axes. 5) 9-fold symmetry was applied. This procedure allowed for the superposition of the doublets/triplets and their associated structures around the 9-fold axis. Steps 1-3 and final visualization were done visually using Chimera (Pettersen et al., 2004). Steps 4 and 5 were done using command line implementations of EMAN2 (7).

TEM

Adult mouse eyes were dissected in a fixation solution (2% paraformaldehyde/2% glutaraldehyde/0.05% CaCl2) and immersion fixed for an additional 1 hour in the same fixative. 150 µm vibratome sections were first stained in 1% tannic acid/0.5% saponin in 0.1M HEPES, pH 7.4 for 1 hour then in 1% uranyl acetate (in 0.1M maleate buffer) for 1 hour each. Sections were then dehydrated with ethanol and embedded with Ultra Bed Epoxy Resin (similar to the embedding detailed in STORM IHC section). 60 – 80 nm ultrathin sections were collected on 100 mesh copper grids (EMS). Grids were post-stained with 1% uranyl acetate and Sato's lead. Imaging was performed on a Hitachi H-7500 TEM.

Antibodies and Labeling Reagents

Primary antibody descriptions, including validation references are described in Table S2. The BBS5 antibody was validated via immunofluorescence in knockout mouse tissue (Fig. S8A-B). 10 µg of wheat germ agglutinin conjugated to Alexa 647 (Molecular Probes) was used as in immunostaining procedures for glycoprotein labeling of mouse retinas.

Confocal Immunohistochemistry and Imaging

All antibodies and labeling reagents used for immunofluorescence were verified for positive signal with confocal microscopy (Fig. S4F). For cryofixation, mouse eye cups were embedded in Optimal Cutting Temperature (OCT) media and plunged into freezing isopentane (i.e. 2-Methlybutane, Sigma) to cryo-fix for 30 minutes before cryosectioning at 8 µm thickness. Alternatively (for tissue used in Fig. S8A-B), WT mouse eyes were embedded in OCT unfixed, and frozen on a floating liquid nitrogen platform; then, unfixed cryosections were post-fixed immediately after sectioning with 1% paraformaldehyde (PFA) for 2 minutes. Sections were blocked in 2% Normal Goat Serum (NGS, Fitzgerald Industries) + 2% Fish Scale Gelatin (Sigma) + 2% Bovine Serum Albumin (Sigma) + 0.2% Triton X-100 dilute in 1x PBS and probed with 0.5 - 1 µg of primary antibody at room temperature overnight. After secondary antibody labeling with goat anti-mouse IgG-Alexa 488 (Thermo Fisher) and/or goat anti-rabbit IgG-Alexa 555 (Thermo Fisher) (1:500),

sections were mounted with Vectashield (Vector Laboratories) for imaging on a Leica TCS-SP5 confocal microscope.

STORM Immunohistochemistry and Resin Embedding

Retinas from either WT or *Bbs* mutant mice were immunolabeled for STORM in a modification of whole mount staining, in which whole retina were stained in solution following a two-step protocol. First, retinas were dissected unfixed in ice cold Ames' media (Sigma) and immediately blocked in 10% NGS (Fitzgerald Industries) + 0.3% saponin (Sigma) + 1x Protease Inhibitor Cocktail (GenDepot) diluted in 1x Ames' media for 2 hours at 4°C. Unfixed labeling of the retina is necessary for complete antibody penetration of the connecting cilium axoneme. Primary antibodies (5-10 µg each) were added to the blocking buffer and incubated at 4°C for 20-22 hours. Retinas were washed 3 times for 5 minutes in 2% NGS in Ames' media on ice before secondary antibodies were added to the same buffer and incubated at 4°C for 2 hours. Additional post-primary washing steps (6 washes for 10 minutes each) helped eliminate excess acetylated alpha-tubulin (acTub) immunolabeling. Secondary antibodies used (8 µg each): F(ab')2-goat anti-mouse IgG Alexa 647 & F(ab')2-goat anti-rabbit IgG Alexa 555 (Thermo Fisher). In WGA-Alexa647 labeling experiments, F(ab')2-goat anti-rabbit IgG Alexa 555 (Thermo Fisher) was used for dual labeling. Retinas were washed in 2% NGS/Ames 6 times for 5 minutes each on ice and fixed in 4% formaldehyde diluted in 1xPBS for 15 minutes at room temperature.

Next, retinas were re-blocked in 10% normal goat serum + 0.2% Triton X-100 diluted in 1xPBS for 2 hours at room temperature. Primary antibodies (5-10 µg each) were

re-added to the blocking buffer and incubated for 2 days at 4°C. This second IHC step features Triton permeabilization to assure complete antigen binding in and around the connecting cilium. After the second primary antibody incubation, retinas were washed 4x for 10 minutes each in 2% NGS/1x PBS. Again, additional washes (8 washes for 10 minutes each) at this step removed excess acTub antibody staining. The same secondary antibodies were added to the wash buffer as before (8 µg each) for overnight incubation at 4°C. Retinas were washed 6x in 2% NGS/1x PBS for 5 minutes each before postfixation in 3% formaldehyde diluted in 1x PBS for 1 hour at room temperature.

The resin embedding protocol for immunolabeled retinas is based on (10-12). Post-fixed retinas were dehydrated in a series of ethanol washes (15 minutes each: 50%, 70%, 90%, 100%, 100%) followed by embedding steps of increasing concentrations with Ultra Bed Epoxy Resin (Electron Microscopy Sciences) to ethanol (2 hours each: 25%:75%, 50%:50%, 75%:25%, 100% resin twice). Embedded retinas were cured on the top shelf of a 65'C baking oven for 20 hours. 500 nm - 1 micron sections were cut on a UCT or UC6 Leica Ultramicrotome and dried directly onto glass-bottom dishes (MatTek 35 mm dish, No. 1.5 coverslip)

STORM Image Acquisition

Immediately prior to imaging, 10% sodium hydroxide (w/v) was mixed with pure 200-proof ethanol for 30 minutes to prepare a mild sodium ethoxide solution. Glass-bottom dishes with ultra-thin retina sections were immersed for 30-40 minutes for chemical etching of the resin that facilitates STORM in embedded tissue (12). Etched sections were then washed and dried on a 50°C heat block. The following STORM

imaging buffer was prepared fresh for each dish: 45 mM Tris (pH 8.0), 9 mM NaCl, oxygen scavenging system: 0.7 mg•ml−1 glucose oxidase (Amiresco) + 42.5 µg ml−1 catalase (Sigma), 10% (w/v) glucose + 100 mM MEA (i.e. L-cysteamine, Chem-Impex) + 10% VECTASHIELD (Vector Laboratories). Imaging buffer was added onto the dried, etched sections and immediately sealed with a second number 1.5 coverslip for imaging.

Imaging was performed on the Nikon N-STORM system, which features a CFI Apo TIRF 100x oil objective (NA1.49) on an inverted Nikon Ti Eclipse microscope that houses a quad cube filter (Chroma, zt405/488/561/640 m-TRF) and a piezo Z stage with Nikon's Perfect Focus System for Z stability. An Agilent MLC400B laser combiner with AOTF modulation housed the 200 mW 561 nm and 647 nm solid-state lasers that were used for imaging in this study. STORM image acquisition was controlled by NIS-Elements Ar software. For each STORM acquisition, a 512x512 pixel field was captured by an Andor iXON DU 897 EMCCD camera (pixel size = 160 nm wide for roughly a 40 square micron STORM area), and a cylindrical lens was inserted into the light path (see below). Chromatic aberration between channels was corrected via X-Y warp calibration, which was performed using a field of view (FOV) of 100nm Tetraspeck beads that were then localized via 2D and 3D STORM acquisitions. A warp function is calculated based on the measured chromatic aberration at the camera, as well as chromatic aberration differences across the FOV, which varies.

The etched thin sections were first scanned with low laser power to locate a region with multiple and sufficiently bright CC. From this region, DIC images and low power laser images (widefield fluorescence images) were saved for reference. To begin a STORM acquisition, both the 561 nm and 647 nm laser lines were increased to maximum power

to photobleach the fluorescence and initiate photoswitching. Images before and after fluorescence photobleaching are shown in Fig, S1A. Reconstructions were compared with and without exclusion of the first 3,500 frames from the STORM acquisition to test for effects of any unquenched fluorophores at the beginning of the acquisitions. The results revealed that any effects were minor effect (Fig S2A). Using an independent power meter, maximum laser power was measured directly above the objective as 34.8 mW for 561 nm (power density = 2.18 kW/cm^2) and 65.5 mW for 647 nm (power density = 4.09 kW/cm^2). Imaging frames were collected at ~56 frames per second. 20,000 - 50,000 frames were collected for each imaging experiment. 561 nm & 647 nm frames were collected sequentially without any lower wavelength "activation" light (a STORM protocol previously termed direct-STORM or dSTORM).

STORM Image Analysis

2D-STORM Analysis of STORM acquisition frames was performed using NIS Elements Ar Analysis software. Drift correction is performed using an auto-correlation algorithm that assesses all stochastic localizations from an acquisition, frame by frame, and fits a calculated drift. Analysis identification settings were used for detection of the individual point spread function (PSF) of photoswitching events in frames from both channels to be accepted and reconstructed as 2D Gaussian data points. The usual settings used for in the analysis for the STORM data (termed "single molecule") are as follows: Minimum PSF height: 400, Maximum PSF height: 65,636, Minimum PSF Width: 200 nm, Maximum PSF Width: 400 nm, Initial Fit Width: 300 nm, Max Axial Ratio: 1.15,

Max Displacement: 1 pixel. These stringent screening parameters yielded predominantly single-molecule positions.

An additional analysis mode termed “centroid” was used for acTub and centrin-2 STORM reconstructions with the following settings: Minimum PSF height: 400, Maximum PSF height: 65,636, Minimum PSF Width: 200 nm, Maximum PSF Width: 700 nm, Initial Fit Width: 300 nm, Max Axial Ratio: 2.5, Max Displacement: 1 pixel. These settings yielded localizations that included single molecule events, both in and out of focus, as well as centers of overlapping double-molecule events. These reconstructions artificially narrowed the profile along the diameters of the cilia but gave an accurate demarcation of the central axis with a sufficiently high spatial sampling frequency to allow accurate computational straightening and alignment of single-molecule reconstructions with respect to the centers of the axonemes. The centroid reconstructions of acTub/centrin-2 were superimposed with corresponding single molecule reconstructions of cilium antigens in the other channel as displayed in most of the STORM figures in this manuscript. These centroid reconstructions were not used for measurements of acTub and centrin-2 distributions, which were all made using “single molecule” reconstructions of those antigens. 3D-STORM via astigmatism was not successful in our samples due to background inherent to our tissue preparation, which rendered poor Z localization.

After analysis, reconstruction quality of “single molecule” STORM data was assessed by plotting Gaussian localization accuracy based on the Thompson equation (13). For each reconstructed connecting cilium Gaussian cluster (defined as a selected ROI surrounding a connecting cilium and surrounding structures), the minimum photon filter values were occasionally increased or decreased and a local density filter (typically

set to 5-10 molecule thresholding value at a 50 nm radius) was used to eliminate background localizations to attain an average localization accuracy in the range of 15–30 nm in each reconstruction, which was used a benchmark for good STORM reconstruction and acceptable background. Reconstructions were processed in Fiji/ImageJ, and the Straighten tool was applied to straighten curved or bent cilia using centroid reconstructions of acTub or centrin to acquire accurate length profiles. Look up table (LUT) settings for visualization within the analysis software were removed from all reconstructions to limit the saturation of strong Gaussians; however, whole image contrast was adjusted for clarity when necessary.

In Fiji/ImageJ, ROI's of digitally straightened STORM reconstructions were measured using row average profiling, which plots the average intensity across the width of the ROI for each row of pixels along the length of the ROI. Pixels were converted to nm for accurate scaling. From these row average profiles, the edges of STORM clusters were set as 1/e times the maximum intensity value for any given cluster profile, and distance from center (radius) was measured as the max intensity value for either acTub and centrin-2 CC clusters (the core) to the edge (1/e max) of the STORM cluster of interest. All presented profiles are normalized by area under the curve. All measurements were made in a 1.1 μm longitudinal region just above the basal body that corresponds to the length of the ultrastructural CC and provided as mean ± standard deviation. For distance from center measurements, STORM clusters that extended beyond either the acTub or centrin-2 centroid reconstruction were measured instead of more colocalized clusters. All measurements were rounded to the nearest nanometer to account for several contingent factors that negate sub-nanometer accuracy of reconstructed STORM

clusters, including antibody displacement (antibody “linkage error”). Other factors that affected our measurements include waviness of individual cilia, slight flattening of the structure by the embedding media and convolution with the point-spread function at the edges of measured STORM clusters.

Ripley’s K-function is a calculated metric that reflects the clustering of molecular coordinates (14-17). For STORM data, the function assesses the distance between molecules from a selected region of a reconstruction. On the graphs in Fig S5C, generated from the NIS-Elements software, the x axis is the distance between molecules (nm) and the y axis is number of molecule pairs within a given distance. Sharp rises in the histogram indicate molecule clusters.

The MosaicIA ImageJ plugin (18) was used to perform the spatial interaction analysis in Figure 4. This analysis determines if two coordinate “patterns” or “clusters” (such as from the two STORM channels) are spatially correlated by modeling an interaction potential and testing if that potential is different from a spatially random distribution. Molecule coordinates from individual CC were extracted from the individual channels from the BBS5 + IFT88 (Fig. 4A) and BBS5 + whirlin (Fig. 4B) STORM experiments (single molecule) manually by carefully outlining each CC region, a ~1 μm^2 area, and avoiding unwanted BB localized molecules. From each of these individual CC coordinate lists, the most accurate 100 molecules (sorted for lowest localization accuracy) from each channel were sorted to be used in the analysis. Channel coordinate lists were uploaded to MosaicIA, and the setting “Kernel wt(p)” was changed for each coordinate set based on the estimate provided by the program. The parameterized “Hernquist potential” (ϵ) was selected to extract the Interaction Strength for each coordinate set.

Interaction strength values were compiled and statistically compared using an unpaired t-test (*** = P<0.0001) (Fig. 4C).

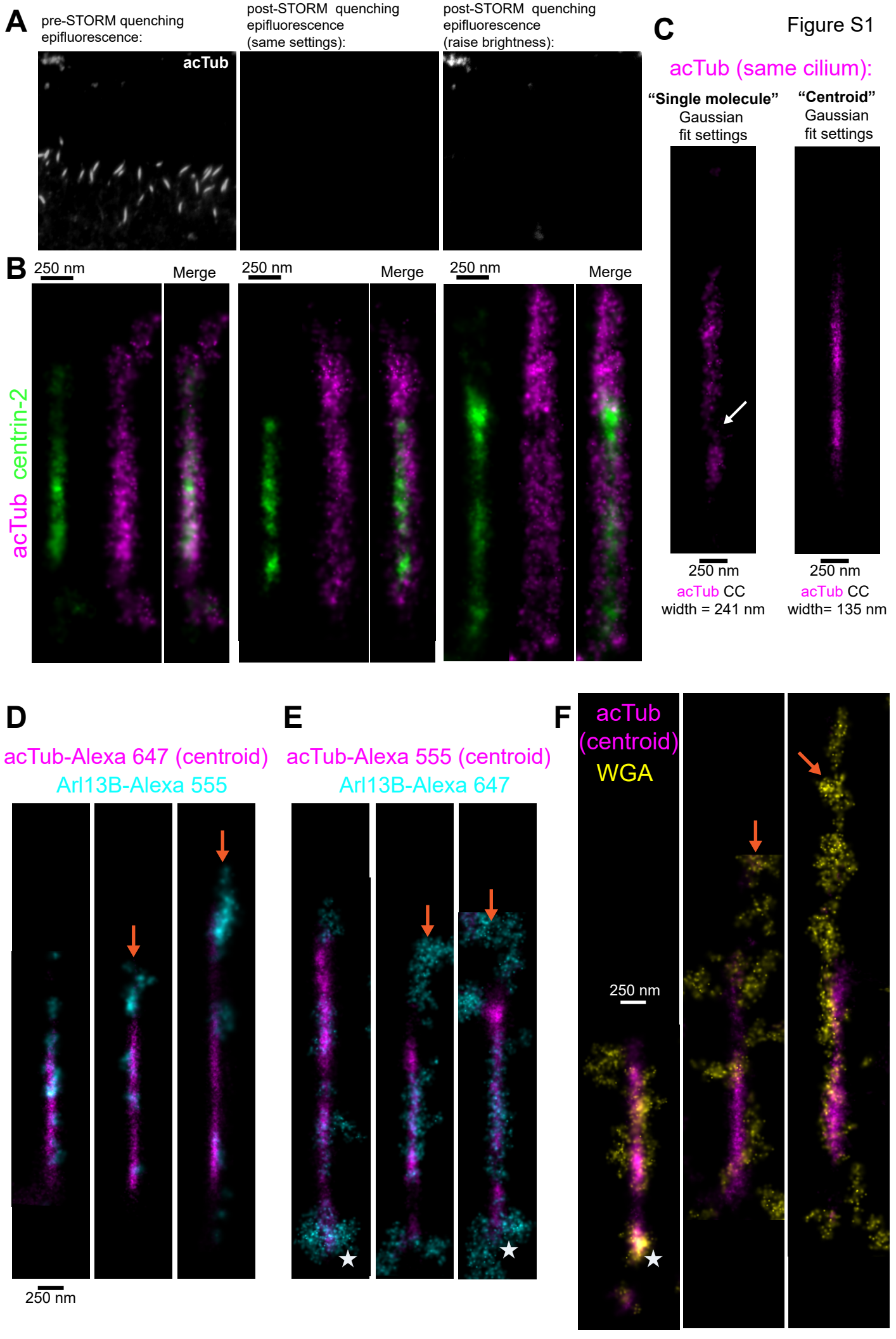
A
pre-STORM quenching epifluorescence:
acTub
post-STORM quenching epifluorescence (same settings):
post-STORM quenching epifluorescence (raise brightness):
B
250 nm
Merge
250 nm
Merge
250 nm
Merge
acTub centrin-2
C
acTub (same cilium):
"Single molecule" Gaussian fit settings
"Centroid" Gaussian fit settings
250 nm
acTub CC width = 241 nm
250 nm
acTub CC width= 135 nm
D
acTub-Alexa 647 (centroid)
Arl13B-Alexa 555
250 nm
E
acTub-Alexa 555 (centroid)
Arl13B-Alexa 647
F
acTub (centroid)
WGA
250 nm

Figure S1. Additional connecting cilia STORM reconstructions of markers for sub-ciliary regions. Reconstructions corresponding to Fig. 2B (B), Fig. 2C (D, E), Fig. 2D (F). (A) Widefield view of acTub fluorescence shown before and after photobleaching, as performed prior to each STORM acquisition. (B) Additional examples of acTub + centrin-2 STORM reconstructions. (C) Comparison of acTub STORM reconstruction applying either the "single molecule" or "centroid" Gaussian fit settings (see SI Methods). White arrow = an under-sampled section of the CC. (D-E) Examples of STORM CC reconstructions from acTub + Arl13B stained tissue with both combinations of Alexa 555 and Alexa 647 labeling each primary antigen to demonstrate the interchangeability of these fluorophores for STORM. (F) Additional CC examples of WGA STORM reconstructions superimposed with acTub centroid reconstructions. Yellow arrows = CC STORM clusters extending to ciliary membrane. Orange arrows = STORM clusters in OS (identified in DIC images). Stars = basal body/inner segment localization.

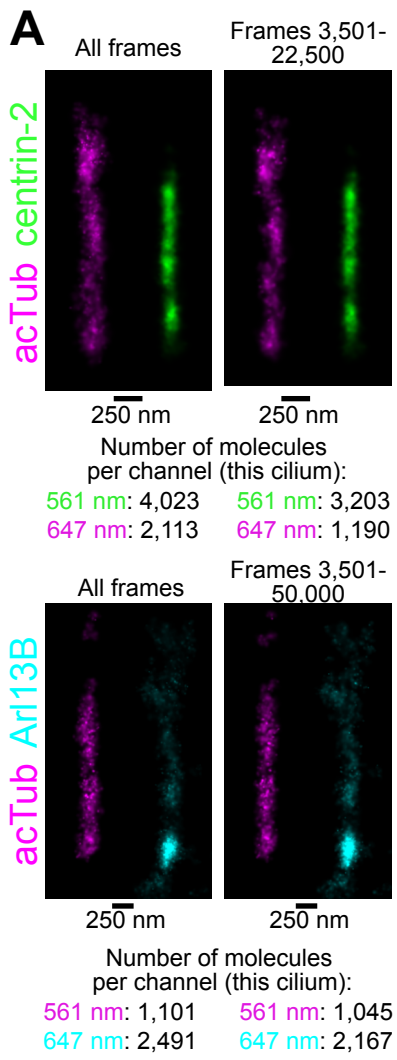
A
All frames
Frames 3,501-22,500
acTub centrin-2
250 nm
250 nm
Number of molecules per channel (this cilium):
561 nm: 4,023
647 nm: 2,113
561 nm: 3,203
647 nm: 1,190
All frames
Frames 3,501-50,000
acTub Arl13B
250 nm
250 nm
Number of molecules per channel (this cilium):
561 nm: 1,101
647 nm: 2,491
561 nm: 1,045
647 nm: 2,167

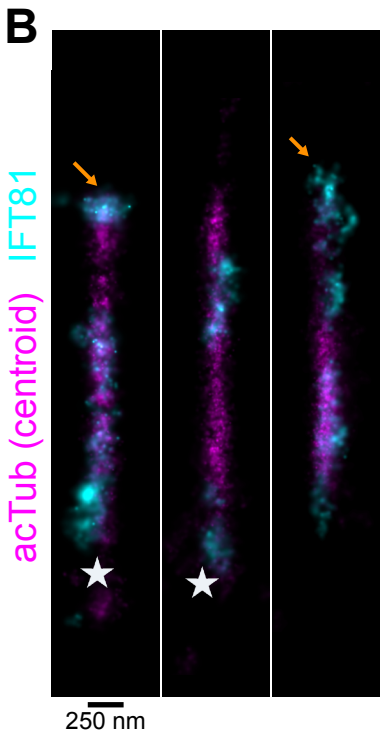
B
acTub (centroid) IFT81
250 nm

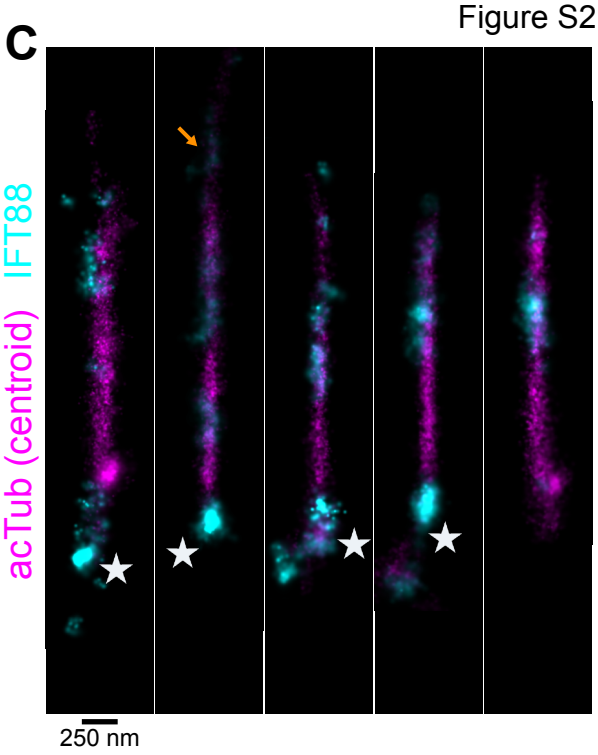
C
acTub (centroid) IFT88
250 nm

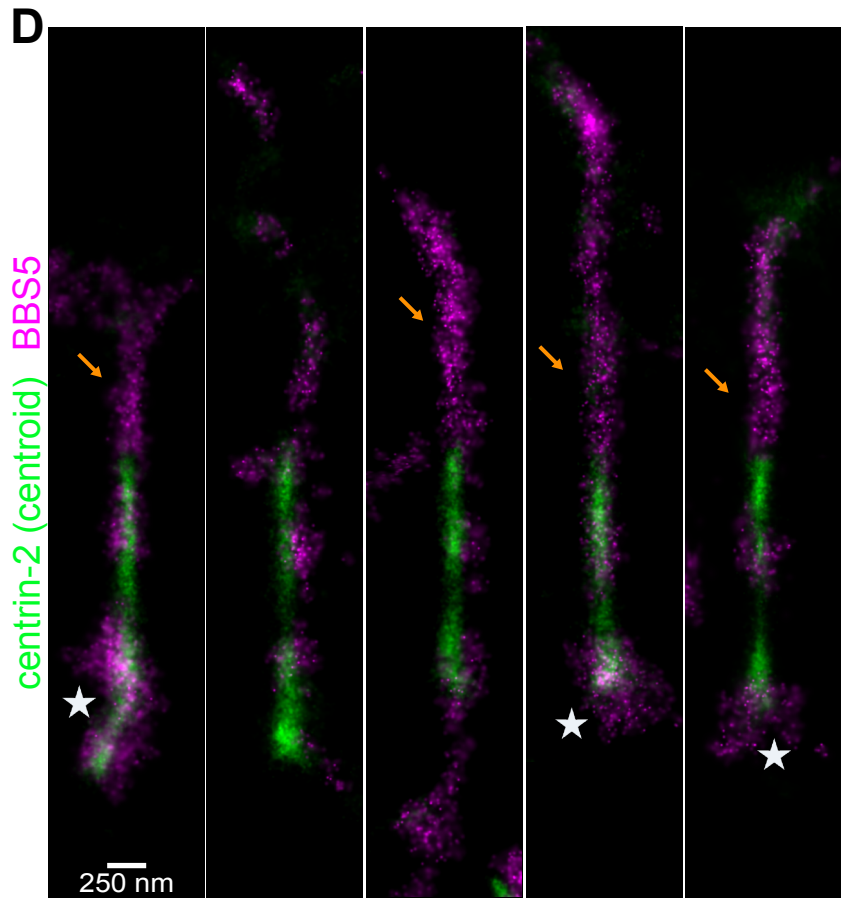
D
centrin-2 (centroid) BBS5
250 nm

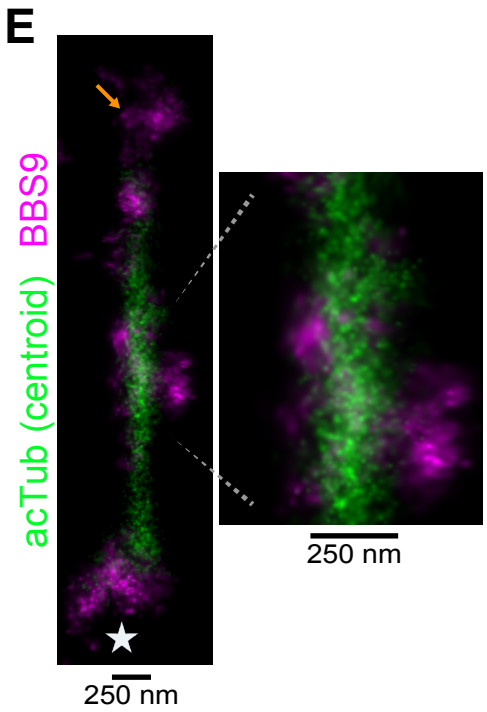
E
acTub (centroid) BBS9
250 nm
250 nm

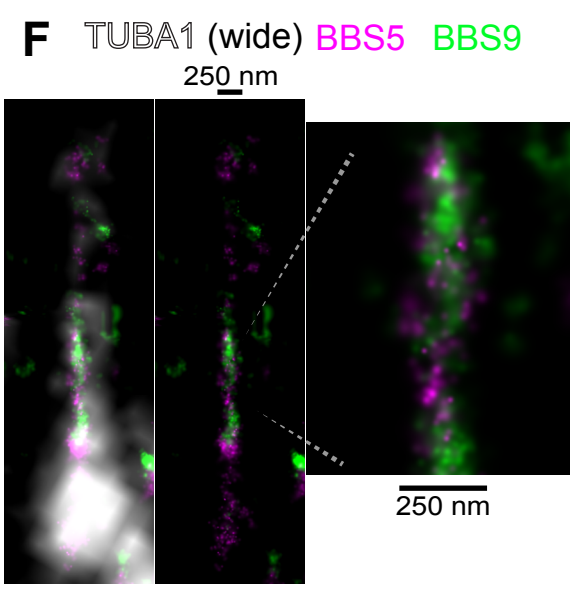
F
TUBA1 (wide) BBS5 BBS9
250 nm
250 nm

Fig. S2. Additional connecting cilia STORM reconstructions of IFT81, IFT88, and BBS5. Replicate reconstructions corresponding to (B) Fig. 3A, (C) Fig. 3B, (D) Fig. 3C. (A) Two sets of CC STORM comparison reconstructions in which either all frames of the STORM acquisition movie are included in the single molecule analysis or the first 3,500 frames are excluded. The two channels are shifted apart horizontally but correctly aligned vertically. Molecule counts per channel are reported corresponding to a ROI containing the depicted cilium. All CC reconstructions and magnifications are of the same scale, respectively, and share the same scale bars. (B) IFT81 and (C) IFT88 STORM reconstructions with centroid reconstructions of acTub superimposed. (D) BBS9 and centrin-2 for (D),(E) are superimposed. Yellow arrows = CC STORM clusters of interest. Orange arrows = OS STORM clusters of interest. Stars = basal body/inner segment STORM clusters. Stars = basal body/inner segment STORM clusters. (E) STORM reconstruction examples of BBS9 (magenta) and acTub (green). (F) STORM reconstruction example of BBS5 (magenta) and BBS9 (green) with corresponding TUBA1 cilia marker (widefield). Magnified view shows overlapped reconstructions.

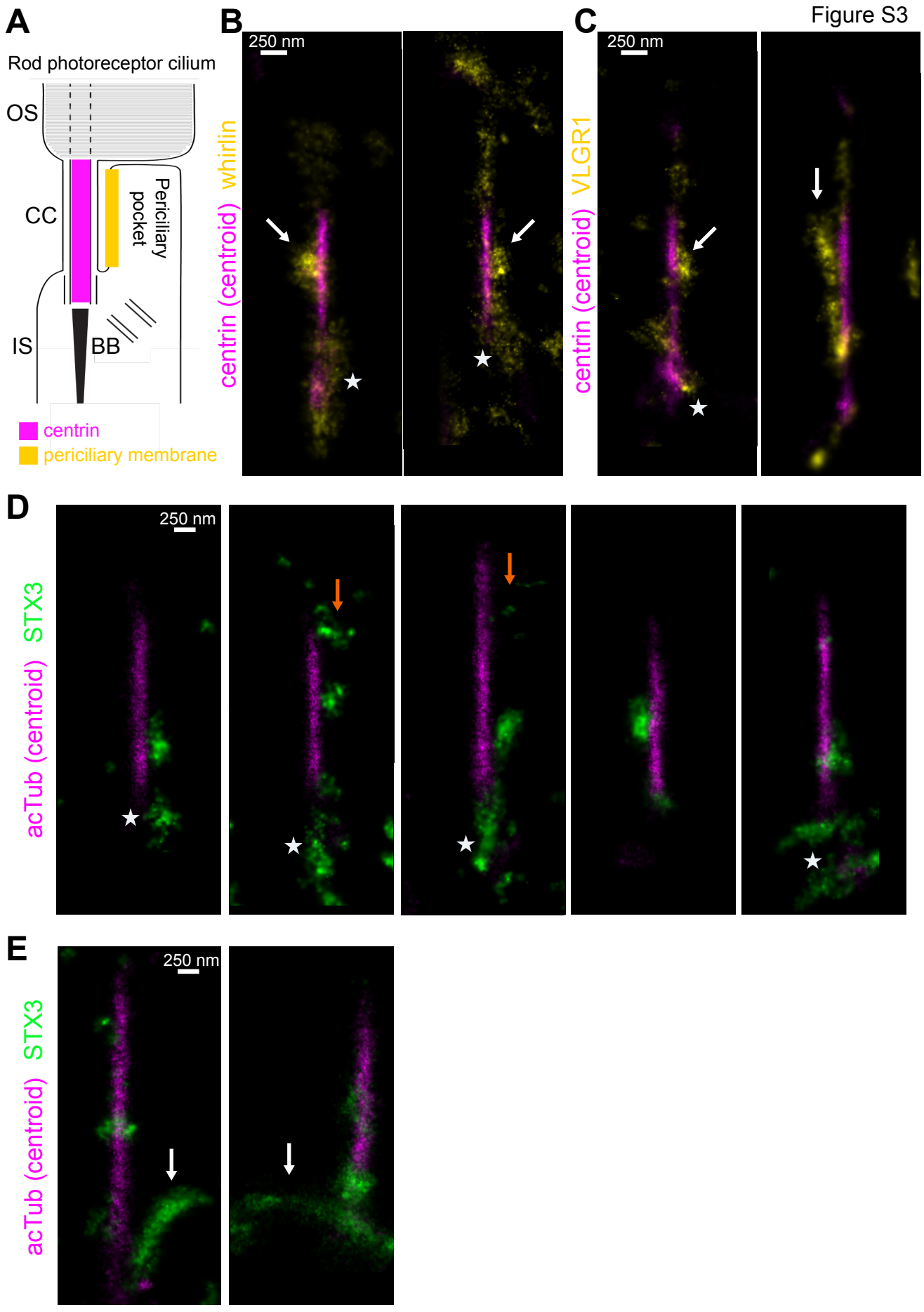
A
Rod photoreceptor cilium
OS
CC
Periciliary pocket
IS
BB
centrin
periciliary membrane
B
250 nm
centrin (centroid) whirlin
C
250 nm
centrin (centroid) VLGR1
D
250 nm
acTub (centroid) STX3
E
250 nm
acTub (centroid) STX3

Fig. S3. Additional connecting cilia STORM reconstructions of whirlin, VLGR1 and STX3. (A) Diagram of rod photoreceptor cilium with corresponding markers for the centrin localization (magenta) and the periciliary membrane (yellow). (B, D) Reconstructions of replicate CC corresponding to Fig. 3D (B, whirlin, yellow) and Fig. 4E (D, STX3, green). (C) STORM reconstruction examples of VLGR1 (yellow) with corresponding centrin (pan-centrin antibody, magenta) centroid reconstruction. In (B) and (C), white arrows indicate periciliary localizations on one side of, and mostly non-overlapping with centrin. All CC reconstructions and magnifications are of the same scale, respectively, and share the same scale bars. Orange arrows = OS STORM clusters of interest. Stars = basal body/inner segment STORM clusters. Stars = basal body/inner segment STORM clusters. (E) acTub (centroid) + STX3 STORM reconstructions in which STX3 clusters are localized far from the axoneme (white arrows); potentially within the periciliary pocket.

Figure S4

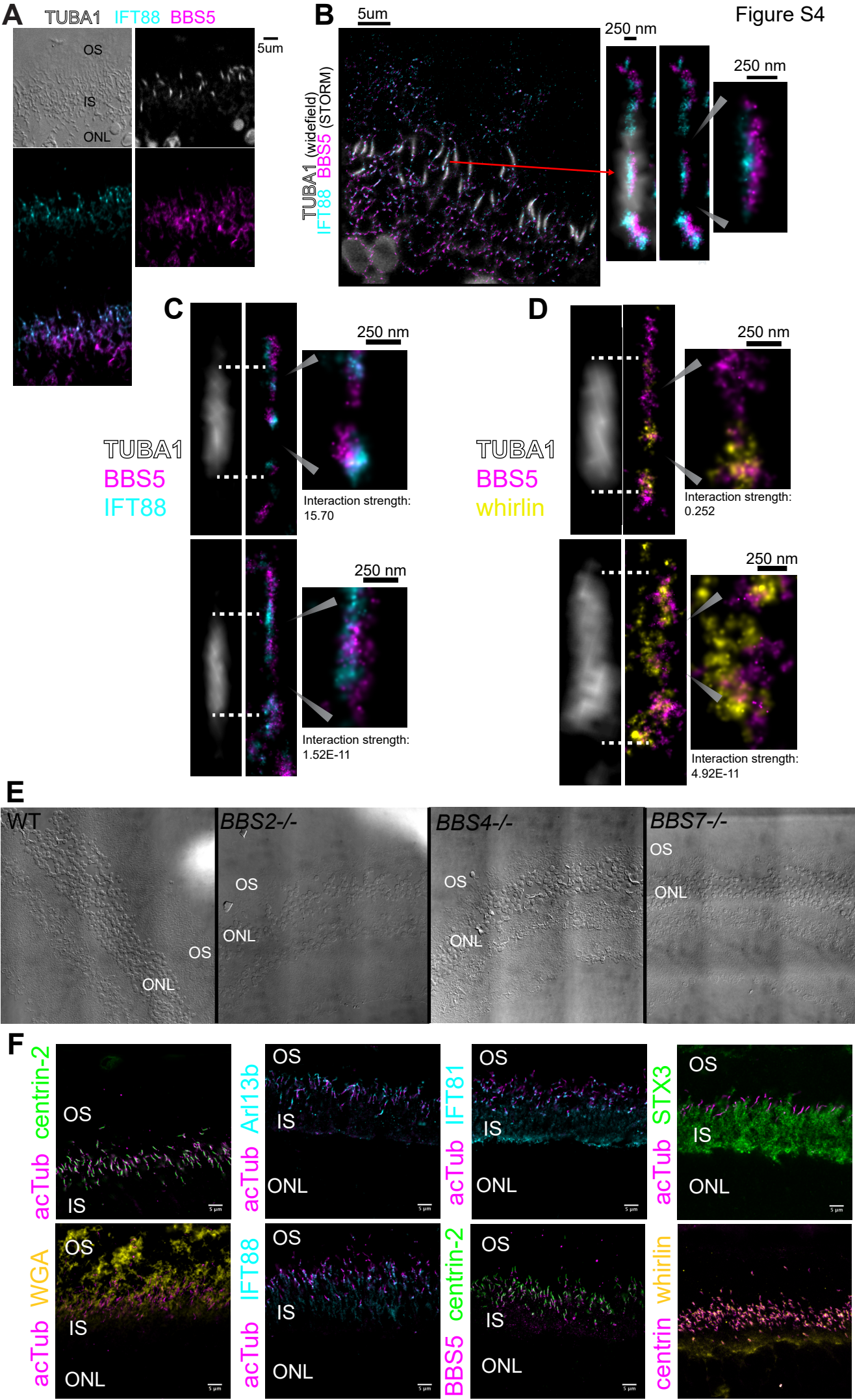
A
TUBA1 IFT88 BBS5
OS
IS
ONL
5um
B
5um
TUBA1 (widefield)
IFT88 BBS5 (STORM)
250 nm
250 nm
C
250 nm
TUBA1
BBS5
IFT88
Interaction strength:
15.70
250 nm
Interaction strength:
1.52E-11
D
250 nm
TUBA1
BBS5
whirlin
Interaction strength:
0.252
250 nm
Interaction strength:
4.92E-11
E
WT
BBS2-/-
BBS4-/-
BBS7-/-
OS
ONL
F
acTub centrin-2
acTub Arl13b
acTub IFT81
acTub STX3
acTub WGA
acTub IFT88
BBS5 centrin-2
centrin whirlin
OS
IS
ONL

Fig. S4. Additional co-localization STORM reconstructions and controls. (A) DIC and widefield fluorescence of a TUBA1 + IFT88 + BBS5 3-color immunostained mouse retina thin section. (B) STORM reconstruction with the same labeling scheme as in (A) overlaid with the TUBA1 widefield image to mark CC boundaries. A single CC is isolated and magnified (red arrow). The colocalization pattern of IFT88 and BBS5 is further magnified to the right. (C) Replicate STORM reconstructions corresponding to Fig. 4A. (D) Replicate reconstructions corresponding to Fig. 4B. Interaction strengths are listed beneath each magnified image in (C) and (D). (D) DIC images of WT and three *Bbs* mutant retinas (*Bbs2-/-, Bbs2-/-, Bbs2-/-*), showing partial preservation of OS at 8 weeks post-natal. (E) Confocal fluorescence images of mouse retina cryosections for antibodies and labeling reagents used for immunostaining and STORM in this study.

Figure S5

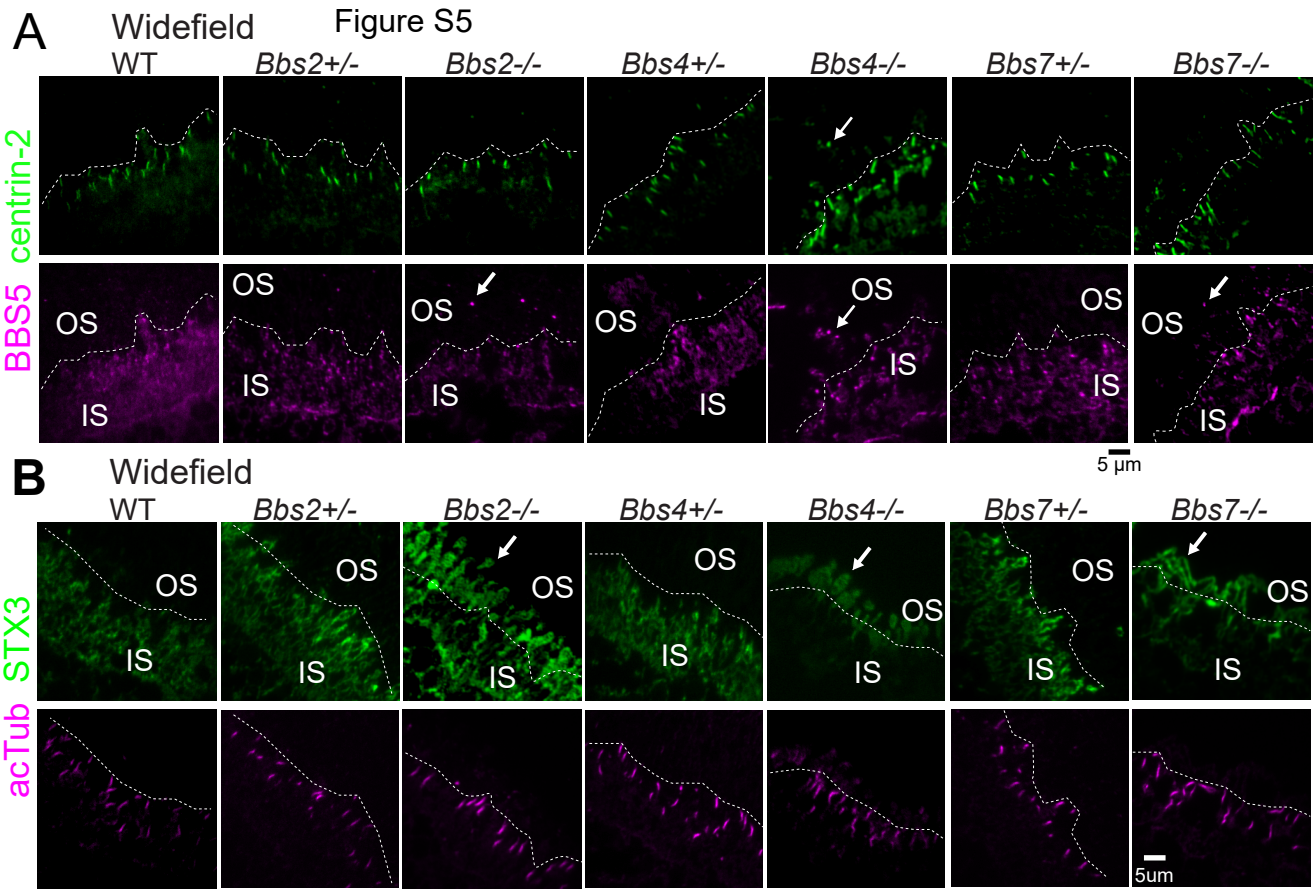
A
Widefield
WT
Bbs2+/-
Bbs2-/-
Bbs4+/-
Bbs4-/-
Bbs7+/-
Bbs7-/-
centrin-2
BBS5
OS
IS
5 µm

B
Widefield
WT
Bbs2+/-
Bbs2-/-
Bbs4+/-
Bbs4-/-
Bbs7+/-
Bbs7-/-
STX3
acTub
OS
IS
5um

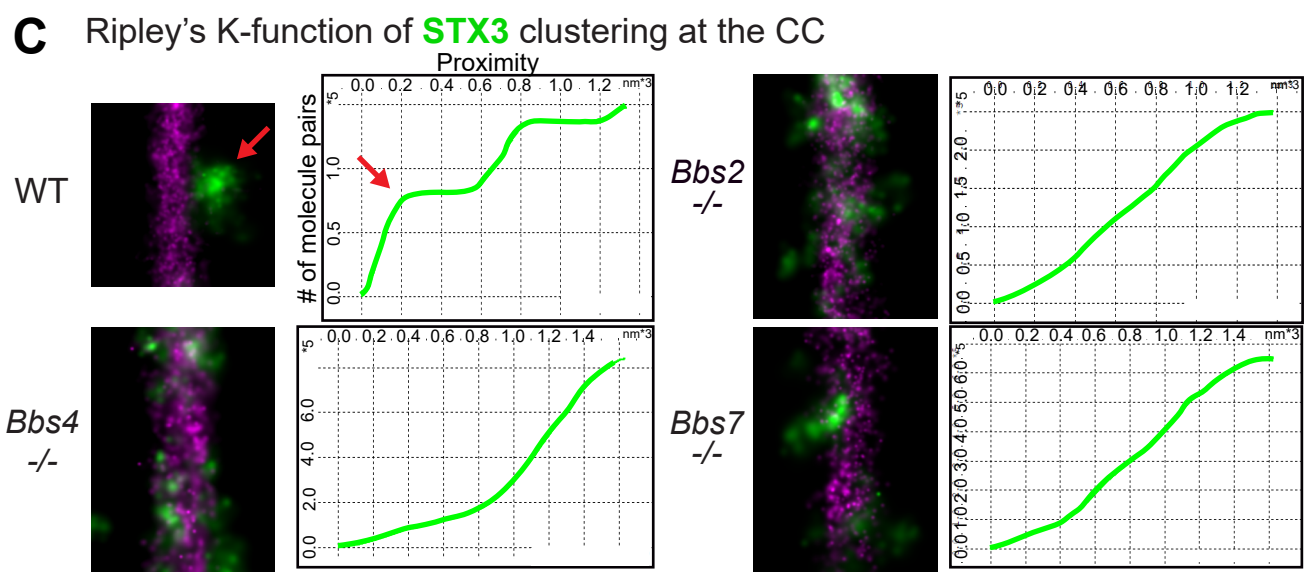
C
Ripley's K-function of STX3 clustering at the CC
Proximity
# of molecule pairs
WT
Bbs2 -/-
Bbs4 -/-
Bbs7 -/-
nm^3

Fig. S5. Effects of BBS deficiencies on BBS5 and syntaxin-3 localization. (A, B) Widefield immunofluorescence of BBS5 (A), centrin 2 (A), acTub (B) and STX3 (B) in WT and *Bbs* mutant mice. Ages for mutant mice: *Bbs2+/-* & *Bbs2-/-* = 8 weeks, *Bbs4+/-* = 8 weeks, *Bbs4-/-* = 5 weeks, *Bbs7+/-* and *Bbs7-/-* = 8 weeks. A dashed line is traced above the acTub positive connecting cilia (CC) to mark the boundary between outer segment (OS) and inner segment (IS). All images are of the same scale and share the same scale bar. White arrows = mislocalizations to the OS in knockout examples. ((C) Ripley's K-function analysis of adjacent example STX3 STORM reconstruction clustering in WT and Bbs mutants reveals a more diffuse distribution within the CC in the mutants. Red arrow indicates sharp incline in the K-function plot due to significant molecule clustering in the corresponding STX3 reconstructions.

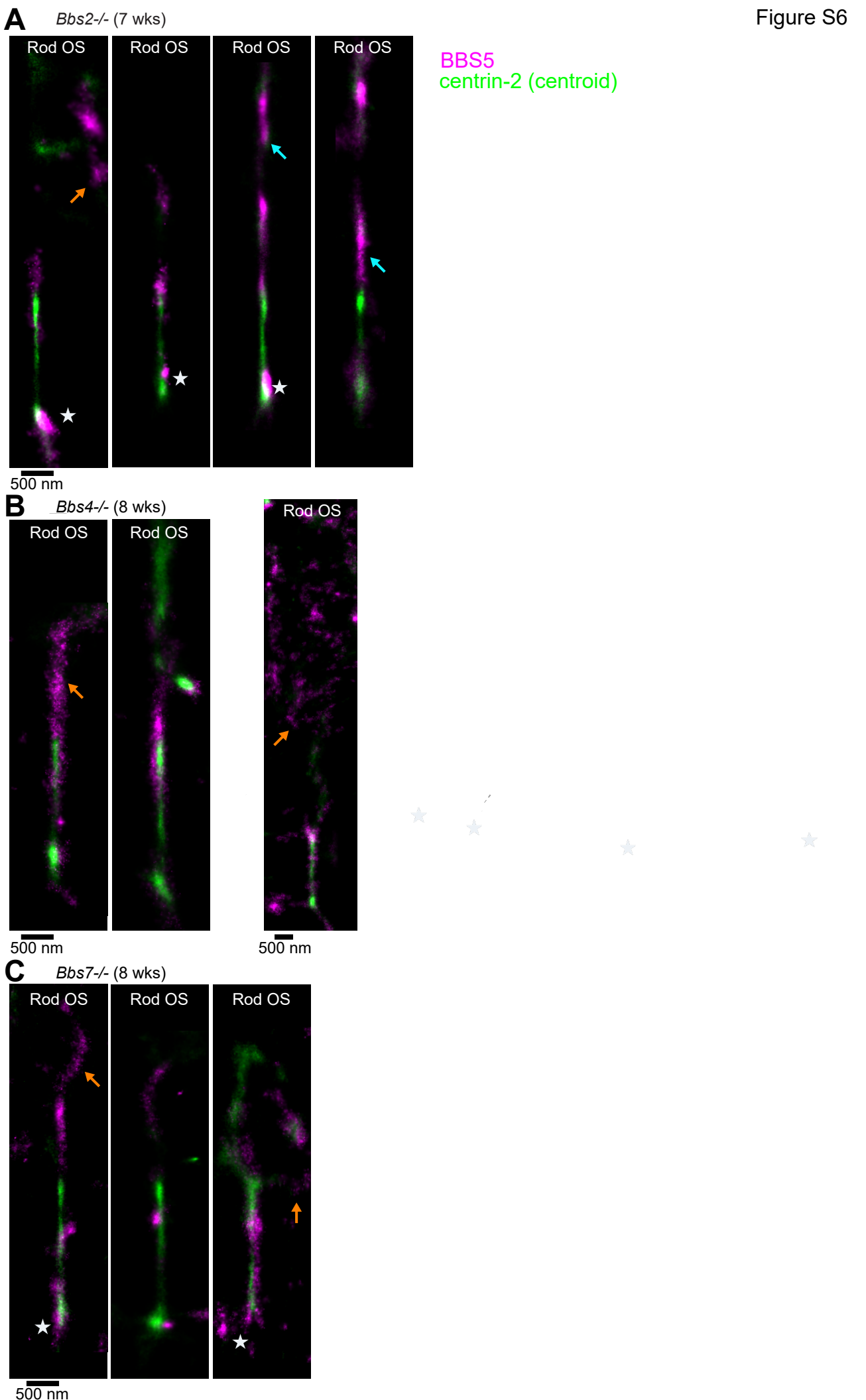
A
Bbs2-/- (7 wks)
Rod OS
Rod OS
Rod OS
Rod OS
BBS5
centrin-2 (centroid)
500 nm
B
Bbs4-/- (8 wks)
Rod OS
Rod OS
Rod OS
500 nm
500 nm
C
Bbs7-/- (8 wks)
Rod OS
Rod OS
Rod OS
500 nm

Fig. S6. Additional STORM reconstructions for BBS5 and centrin-2 in *Bbs* mutant rod photoreceptors. All Bbs mutant CC examples are from age 7-8 week mice (A-C). Rod outer segment ("Rod OS") STORM examples from a wider view are depicted to include the OS and demonstrate mislocalization there. White stars = BB/IS STORM clusters. Orange arrows = aberrant BBS5 localization in the OS. Cyan arrows = normal BBS5 localization in the OS.

Figure S7

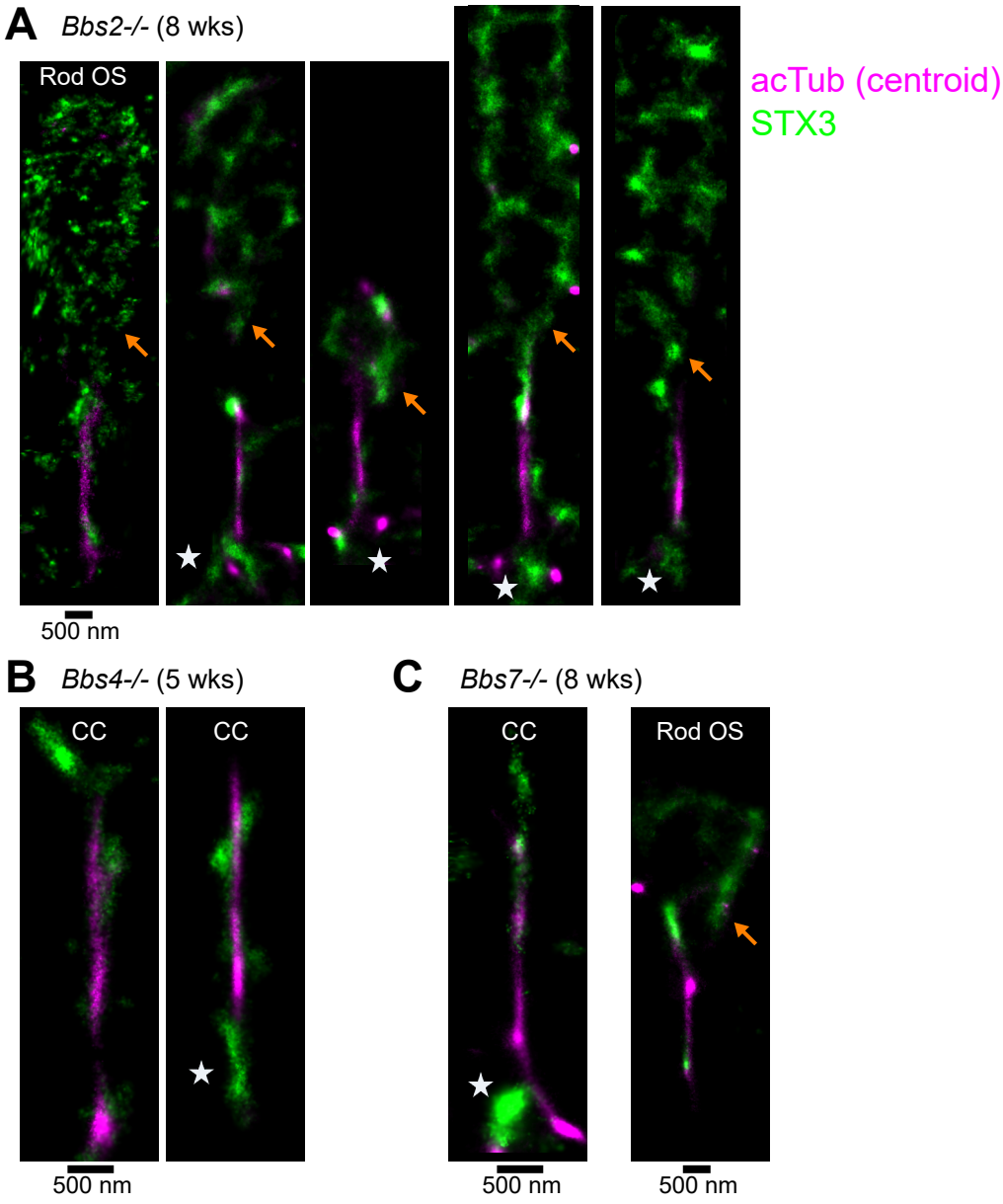
A
Bbs2-/- (8 wks)
Rod OS
acTub (centroid)
STX3
500 nm
B
Bbs4-/- (5 wks)
CC
CC
500 nm
C
Bbs7-/- (8 wks)
CC
Rod OS
500 nm
500 nm

Fig. S7. Additional STORM reconstructions for STX3 and acTub in *Bbs* mutant rod photoreceptors. (A) *Bbs2-/-*, (B, C) *Bbs4-/-*, (D) *Bbs7-/-*. Ages are as indicated. White stars = BB/IS STORM clusters. Orange arrows = STX3 mis-accumulation in the OS.

Figure S8

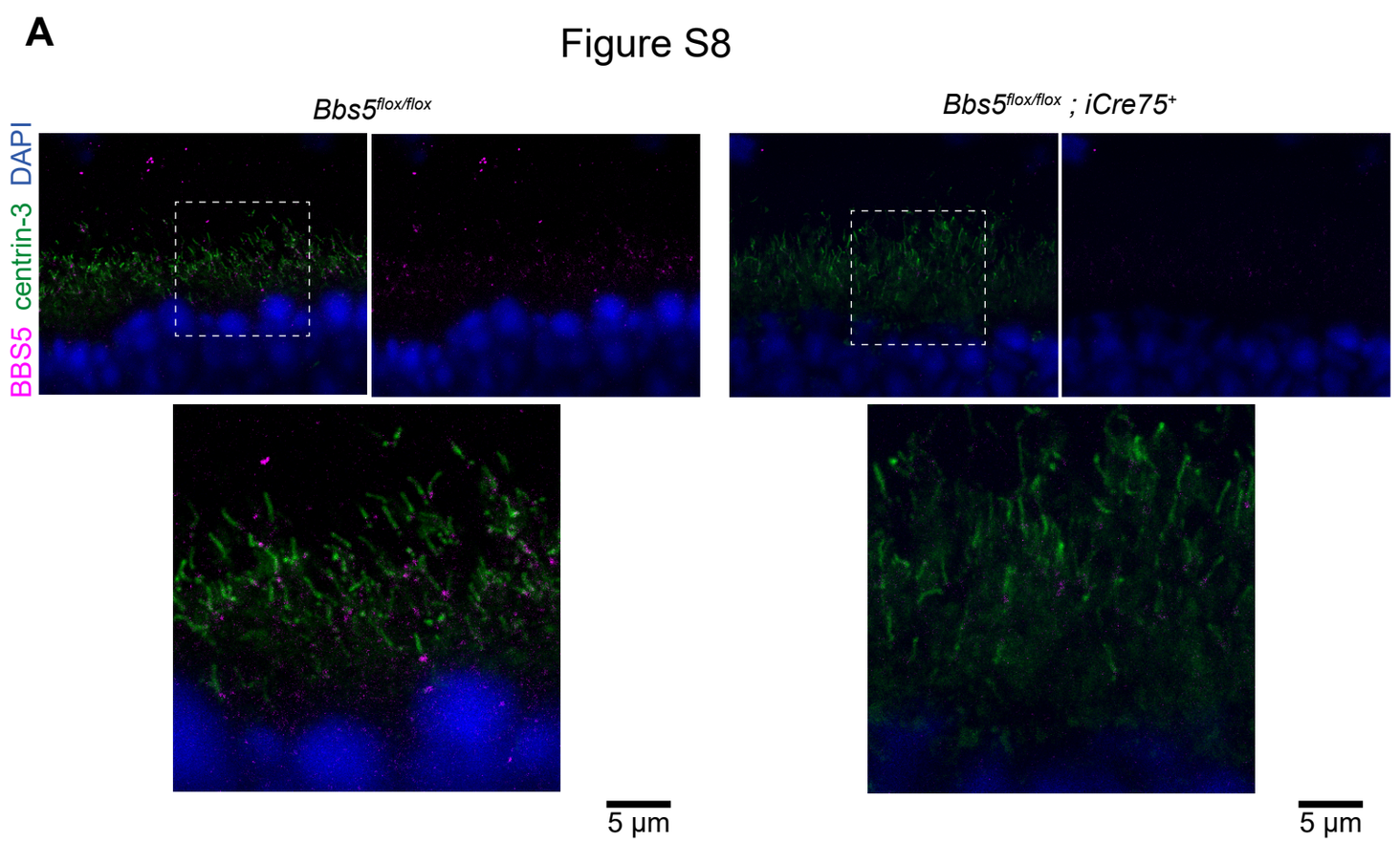
A
Bbs5flox/flox
Bbs5flox/flox ; iCre75+
BBS5 centrin-3 DAPI
5 µm
5 µm

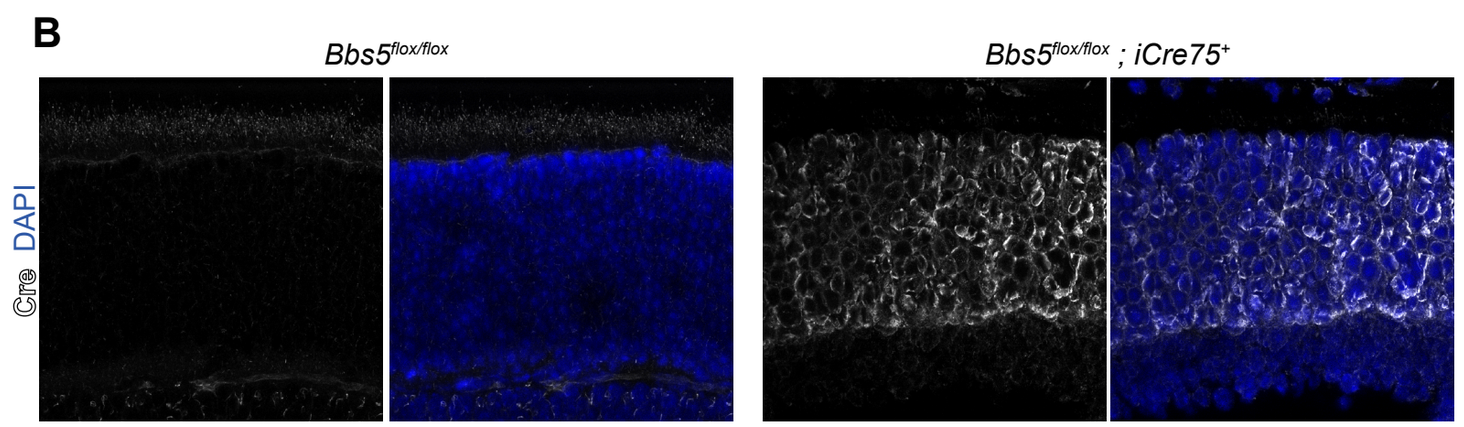
B
Bbs5flox/flox
Bbs5flox/flox ; iCre75+
Cre DAPI

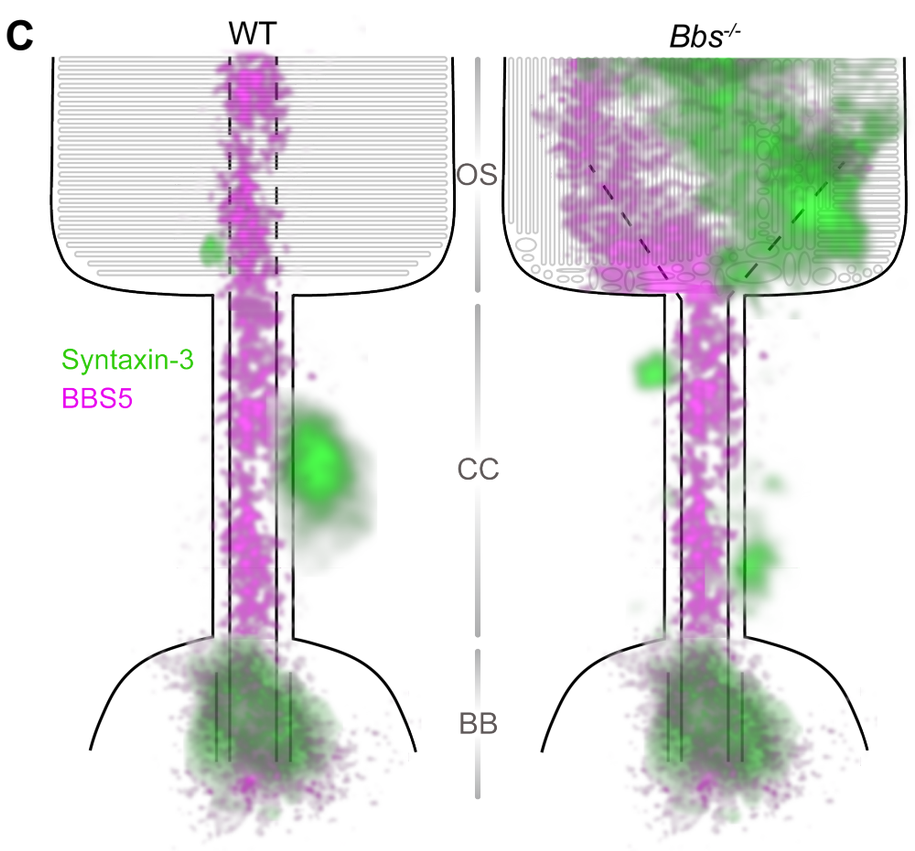
C
WT
Bbs-/-
OS
CC
BB
Syntaxin-3
BBS5

Fig. S8. Validation of BBS5 antibody specificity. (A) Cryosections of retinas from BBS5flox/flox conditional knockout mouse littermates (age 4 weeks) are compared with or without Cre expression in rod cells (iCre75+). Bright BBS5 positive puncta that are brighter than background signal are missing in the iCre75+ knockout retina, validating the specificity of BBS5 antibody immunolabeling. (B) Cre immunofluorescence confirms Cre expression in the outer nuclear layer of the iCre75+ mouse only. Background staining in other retina layers is comparable in both genotypes. (C) Model of the super-resolution localization of syntaxin-3 and BBS5 in WT and Bbs-/- rod cilia. Syntaxin-3 (STX3, green), BBS5 (magenta).

Table S1. List of biological replicates and cilia samples for each IF experimental condition.

Genotype	IF antibodies	Related Figures	# Biological mouse replicates	# Cilia analyzed with STORM
WT	α Acetylated alpha-tubulin + α Centrin-2	Figure 2B, Figure S1B-C	**3**	**17**
WT	α Acetylated alpha-tubulin + α Arl13B	Figure 2C, Figure S1D-E	**3**	**23**
WT	α Acetylated alpha-tubulin + WGA	Figure 2D, Figure S1F	**3**	**15**
WT	α Acetylated alpha-tubulin + α IFT81	Figure 3A, Figure S2A	**4**	**9**
WT	α Acetylated alpha-tubulin + α IFT88	Figure 3B, Figure S2B	**5**	**26**
WT	α BBS5 + α centrin-2	Figure 3C, Figure S2C	**2**	**22**
WT	α whirlin + α centrin	Figure 3D, Figure S3B	**4**	**24**
WT	α whirlin + α VLGR1	Figure S3C	**2**	**19**
WT	α Acetylated alpha-tubulin + α BBS9	Figure S2D	**1**	**19**
WT	α TUBA1-ATTO488 + α BBS5 + α BBS9	Figure S2E	**1**	**11**
WT	α TUBA1-ATTO488 + α BBS5 + α IFT88	Figure 4A, Figure S4A-C	**2**	**21**
WT	α TUBA1-ATTO488 + α BBS5 + α whirlin	Figure 4B, Figure S4D	**2**	**63**
WT	α Acetylated alpha-tubulin + α Syntaxin-3	Figure 4D-E, Figure S3D	**2**	**28**
Bbs2-/-	α BBS5 + α centrin-2	Figure 5A, Figure S6A-B	**3** (age 8 wks)	**17**
Bbs2-/-	α Acetylated alpha-tubulin + α Syntaxin-3	Figure 6A, Figure S7A	**3** (age 8 wks)	**12**
Bbs4-/-	α BBS5 + α centrin-2	Figure 5B, Figure S6C-D	**7** [3 (age 5 wks) + 4 (age 8 wks)]	**37** [13 (age 5 wks) + 24 (age 8 wks)]
Bbs4-/-	α Acetylated alpha-tubulin + α Syntaxin-3	Figure 6B, Figure S7B	**5** [2 (age 5 wks) + 3 (age 8 wks)]	**24** [8 (age 5 wks) + 16 (age 8 wks)]
Bbs7-/-	α BBS5 + α centrin-2	Figure 5C, Figure S6C-D	**5** [1 (age 7 wks) + 4 (age 8 wks)]	**38** [8 (age 7 wks) + 30 (age 8 wks)]
Bbs7-/-	α Acetylated alpha-tubulin + α Syntaxin-3	Figure 6C, Figure S7C-D	**4** [2 (age 8 wks) + 2 (age 15 wks)]	**20** [10 (age 8 wks) + 10 (age 15 wks)]

Table S2. List of primary antibodies with supporting information and validation references.

Antigen	Immunogen	Source	Host	Validation Reference
Acetylated alpha-tubulin (6-11B-1)	Acetylated alpha-tubulin from the outer arms of *S. perperatus* sperm axonemes.	Millipore Sigma (T67930) and Santa Cruz Biotechnology (sc-23950)	Mouse monoclonal	(Piperno and Fuller. *JCB*, 1985) [1]
Centrin-2	*H. sapiens* Centrin-2 N-terminus peptide	Santa Cruz Biotechnology (sc-27793-R)	Rabbit polyclonal	Antibody discontinued by manufacturer; (Boutros et al. *Biol Cell*, 2011) [2]
Centrin-2	*H. sapiens* Centrin-2 (aa 1-172)	Proteintech (15877-1-AP)	Rabbit polyclonal	(Fong et al. *Cell*, 2011) [3]
Centrin-3	*H. sapiens* Centrin-2 (aa 1-167)	Proteintech (15811-1-AP)	Rabbit polyclonal	Not validated; Used solely as a cilia marker in Figure S8
Centrin	*Chlamydomonas* Centrin (C-terminus)	Millipore Sigma (04-1624) (clone 20H5)	Mouse monoclonal	(Paoletti et al. *JCS*. 1996)[4]
Cre	n/a	EMD Millipore (69050)	Rabbit polyclonal	This work (Figure S8)
ARL13B	*H. sapiens* ARL13B (aa 1-321)	Proteintech (17711-1-AP)	Rabbit polyclonal	(Humbert et al. *PNAS*, 2012), (Roy et al. *JBC*, 2017) [5,6]
IFT88	*H. sapiens* IFT88 (aa 532 - 833)	Proteintech (13967-1-AP)	Rabbit polyclonal	(Kodani et al. *EMBO*, 2013), (Phua et al. *Cell*, 2017) [7,8]
IFT81	*H. sapiens* IFT81 (aa 550 – 676)	Proteintech (11744-1-AP)	Rabbit polyclonal	Not validated; notably this antibody is used in conjunction with other IFT protein primary cilia immunofluorescence in high impact publications including (Phua et al. *Cell*, 2017), (Yeyati et al. *JCB*, 2017) [8,9]
BBS5	*M. musculus* BBS5 (full length)	(Smith et al, *Cell. Mol. Life Sci,* 2013*)* [10]	Mouse monoclonal	This work (Figure S8). Antibody described in (Smith et al, *Cell. Mol. Life Sci,* 2013)[10]
BBS9	*H. sapiens* BBS9 (aa 47–330)	Santa Cruz Biotechnology (sc-292152)	Rabbit polyclonal	Antibody discontinued by manufacturer
Alpha-tubulin (TUBA1) - ATTO488	Bovine brain tubulin	antibodies-online.com (ABIN4888971)	Human monoclonal	Original unconjugated TUBA1 recombinant human single chain fragment variable (scFV), validated by molecular weight (Nizak et al. *Traffic*, 2003) [11]
Whirlin	*H. sapiens* DFNB31 (aa 558-907)	Proteintech (25881-1-AP)	Rabbit polyclonal	Not validated, but STORM immunolocalization in photoreceptor cells validated by comparing to VLGR localization (this paper).
VLGR1	*M. musculus* VLGER1b (aa 6198-6307)	Gift from Dr. Uwe Wolfrum (U. Mainz, Germany)	Rabbit polyclonal	(Reiners et al. *Human Mol Gen*, 2005)[12] Immunolocalization validation with immuno-EM in (Maerker et al. *Human Mol Gen*, 2008)[13].
Syntaxin-3	*H. sapiens* BBS9 (aa 1–264)	Proteintech (15556-1-AP)	Rabbit polyclonal	Validated by molecular weight (Datta et al. *PNAS*, 2015) [14]; notably this antibody is used extensively in immunofluorescence analyses of *Bbs* mutant mouse retinas (Hsu et al. *PLoS Genetics*, 2017), (Dilan et al. *Hum. Mol. Genet*, 2018) [15,16]

Table 2 References

1. Piperno, G. & Fuller, M. T. Monoclonal antibodies specific for an acetylated form of alpha-tubulin recognize the antigen in cilia and flagella from a variety of organisms. *J. Cell Biol.* **101**, 2085–94 (1985).
2. Boutros, R. *et al.* CDC25B associates with a centrin 2-containing complex and is involved in maintaining centrosome integrity. *Biol. Cell* **103**, 55–68 (2011).
3. Fong, Y. W. *et al.* A DNA repair complex functions as an Oct4/Sox2 coactivator in embryonic stem cells. *Cell* **147**, 120–131 (2011).
4. Paoletti, A., Moudjou, M., Paintrand, M., Salisbury, J. L. & Bornens, M. Most of centrin in animal cells is not centrosome-associated and centrosomal centrin is confined to the distal lumen of centrioles. *J. Cell Sci.* **3102**, 3089–3102 (1996).
5. Humbert, M. C. *et al.* ARL13B, PDE6D, and CEP164 form a functional network for INPP5E ciliary targeting. *Proc. Natl. Acad. Sci.* **109**, 19691–19696 (2012).
6. Roy, K. *et al.* Palmitoylation of the ciliary GTPase ARL13b is necessary for its stability and its role in cilia formation. *J. Biol. Chem.* **292**, 17703–17717 (2017).
7. Kodani, A., Salomé Sirerol-Piquer, M., Seol, A., Manuel Garcia-Verdugo, J. & Reiter, J. F. Kif3a interacts with Dynactin subunit p150 Glued to organize centriole subdistal appendages. *EMBO J.* **32**, 597–607 (2013).
8. Phua, S. C. *et al.* Dynamic Remodeling of Membrane Composition Drives Cell Cycle through Primary Cilia Excision. *Cell* **168**, 264-279.e15 (2017).
9. Yeyati, P. L. *et al.* KDM3A coordinates actin dynamics with intraflagellar transport to regulate cilia stability. *J. Cell Biol.* **216**, 999–1013 (2017).
10. Smith, T. S. *et al.* Light-dependent phosphorylation of Bardet-Biedl syndrome 5 in photoreceptor cells modulates its interaction with arrestin1. *Cell. Mol. Life Sci.* (2013). doi:10.1007/s00018-013-1403-4
11. Nizak, C. *et al.* Recombinant antibodies against subcellular fractions used to track endogenous Golgi protein dynamics in vivo. *Traffic* **4**, 739–753 (2003).
12. Reiners, J. *et al.* Scaffold protein harmonin (USH1C) provides molecular links between Usher syndrome type 1 and type 2. *Hum. Mol. Genet.* **14**, 3933–3943 (2005).
13. Maerker, T. *et al.* A novel Usher protein network at the periciliary reloading point between molecular transport machineries in vertebrate photoreceptor cells. *Hum. Mol. Genet.* **17**, 71–86 (2008).
14. Datta, P. *et al.* Accumulation of non-outer segment proteins in the outer segment underlies photoreceptor degeneration in Bardet–Biedl syndrome. *Proc. Natl. Acad. Sci.* **112**, E4400–E4409 (2015).
15. Hsu, Y. *et al.* BBSome function is required for both the morphogenesis and maintenance of the photoreceptor outer segment. *PLOS Genet.* **13**, e1007057 (2017).
16. Dilan, T. L. *et al.* Bardet–Biedl syndrome-8 (BBS8) protein is crucial for the development of outer segments in photoreceptor neurons. *Hum. Mol. Genet.* **27**, 283–294 (2018).

References

1. J. C. Gilliam *et al.*, Three-dimensional architecture of the rod sensory cilium and its disruption in retinal neurodegeneration. *Cell* **151**, 1029-1041 (2012).
2. T. G. Wensel, J. C. Gilliam, Three-dimensional architecture of murine rod cilium revealed by cryo-EM. *Methods Mol Biol* **1271**, 267-292 (2015).
3. D. N. Mastronarde, Automated electron microscope tomography using robust prediction of specimen movements. *J Struct Biol* **152**, 36-51 (2005).
4. X. Li *et al.*, Electron counting and beam-induced motion correction enable near-atomic-resolution single-particle cryo-EM. *Nat Methods* **10**, 584-590 (2013).
5. J. R. Kremer, D. N. Mastronarde, J. R. McIntosh, Computer visualization of three-dimensional image data using IMOD. *J Struct Biol* **116**, 71-76 (1996).
6. D. N. Mastronarde, S. R. Held, Automated tilt series alignment and tomographic reconstruction in IMOD. *J Struct Biol* **197**, 102-113 (2017).
7. G. Tang *et al.*, EMAN2: an extensible image processing suite for electron microscopy. *J Struct Biol* **157**, 38-46 (2007).
8. E. F. Pettersen *et al.*, UCSF Chimera--a visualization system for exploratory research and analysis. *J Comput Chem* **25**, 1605-1612 (2004).
9. A. Y. Koyfman *et al.*, Structure of Trypanosoma brucei flagellum accounts for its bihelical motion. *Proc Natl Acad Sci U S A* **108**, 11105-11108 (2011).
10. E. Johnson *et al.*, Correlative in-resin super-resolution and electron microscopy using standard fluorescent proteins. *Sci Rep* **5**, 9583 (2015).
11. D. Kim *et al.*, Correlative stochastic optical reconstruction microscopy and electron microscopy. *PLoS One* **10**, e0124581 (2015).
12. Y. M. Sigal, C. M. Speer, H. P. Babcock, X. Zhuang, Mapping Synaptic Input Fields of Neurons with Super-Resolution Imaging. *Cell* **163**, 493-505 (2015).
13. R. E. Thompson, D. R. Larson, W. W. Webb, Precise nanometer localization analysis for individual fluorescent probes. *Biophys J* **82**, 2775-2783 (2002).
14. M. A. Kiskowski, J. F. Hancock, A. K. Kenworthy, On the use of Ripley's K-function and its derivatives to analyze domain size. *Biophys J* **97**, 1095-1103 (2009).
15. S. F. Lee, M. A. Thompson, M. A. Schwartz, L. Shapiro, W. E. Moerner, Super-resolution imaging of the nucleoid-associated protein HU in Caulobacter crescentus. *Biophys J* **100**, L31-33 (2011).
16. D. M. Owen, D. Williamson, A. Magenau, K. Gaus, Optical techniques for imaging membrane domains in live cells (live-cell palm of protein clustering). *Methods Enzymol* **504**, 221-235 (2012).
17. P. Rubin-Delanchy *et al.*, Bayesian cluster identification in single-molecule localization microscopy data. *Nat Methods* **12**, 1072-1076 (2015).
18. A. Shivanandan, A. Radenovic, I. F. Sbalzarini, MosaicIA: an ImageJ/Fiji plugin for spatial pattern and interaction analysis. *BMC Bioinformatics* **14**, 349 (2013).